NUMERICAL COMPARISON OF ONE AND TWO-DIMENSIONAL MODELS FOR NON-NEWTONIAN FLUID HAMMER

Tainan Gabardo Miranda dos Santos, tainansantos@utfpr.edu.br
Gabriel Merhy de Oliveira, gabrielm@utfpr.edu.br
Cezar Otaviano Ribeiro Negrão, negrao@utfpr.edu.br
Research Center for Rheology and Non-Newtonian Fluids (CERNN), Federal University of Technology-Parana (UTFPR), Av. Sete de Setembro, 3165, Curitiba-PR, 80230-901, Brazil

Abstract. *The study of fluid transients is essential when designing pipelines. Transients may be caused by sudden changes in boundary conditions such as the closure of a valve in a fluid hammer problem. The closure causes over pressure and wave propagations that can damage the pipeline causing accidents and leakage. Most works use water or Newtonian oils to study the problem. Nevertheless, non-Newtonian fluids, such as slurries, pastes, swages and suspensions, are also transported. Therefore, this work aims to study the non-Newtonian fluid hammer problem through the numerical simulation of two mathematical models. In these models the flow is considered laminar, weakly compressible, isothermal and the fluid is assumed to behave as a Power Law fluid. The mass and momentum balance equation are solved by the method of the characteristics (MOC). The first model is one-dimensional (1D) and the second is two-dimensional (2D). A comparison is realized in order to evaluate in which conditions the solution of both models converges or diverges. The results show that the 1D model is less dissipative and predicts a lower pressure overshoot when compared to the 2D model. When the fluid is more dissipative, the solution of these models is closer. The effect of the power law index is also studied. As the fluid becomes more pseudoplastic (lower values of the power law index) the dissipation increases and equilibrium is reached ealier. The Richardson annular effect (the presence of a local maximum for the axial velocity near the wall) is more pronounced for shear-thickening fluids.*

Keywords*: fluid transients, fluid hammer, mathematical models, power-law fluid, compressible flow*

1. NOMENCLATURE

A: cross area [m^2]
c: wave speed [$m.s^{-1}$]
C: characteristics line
d: diameter [m]
f: friction factor [-]
g: gravity [$m.s^{-2}$]
h: pressure head [m]
k: consistency index [$Pa.s^n$]
l: length [m]
Ma: Mach number [-]
n: power-law index [-]
NR: number of axial divisions [-]
NZ: number of radial divisions [-]
q: radius times radial local velocity [$m^2.s^{-1}$]
r: radial coordinate [m]
Re: Reynolds number [-]
t: time [s]
T: temperature [K]
v_r: radial local velocity [$m.s^{-1}$]
v_z: axial local velocity [$m.s^{-1}$]
V_z: axial mean velocity [$m.s^{-1}$]
z: axial coordinate [m]
Greeks
α: compressibility [Pa^{-1}]
δ: aspect ratio [-]
$\dot{\gamma}$: shear rate [s^{-1}]
η: apparent viscosity [Pa.s]
ρ: fluid density [$kg.m^{-3}$]
τ: shear stress [Pa]
Subscripts
c: center
in: inlet
out: outlet
w: wall
Subscripts
*: dimensionless
+: characteristics direction
-: characteristics direction

2. INTRODUCTION

Fluid transients are normally caused by sudden changes in boundary conditions, such as the closure or opening of a valve and the shutdown or start of a pump. These abrupt variations can cause increase of the pressure and can damage the overall system. Thus when transporting fluids, it is important to predict these overpressures in order to assure reliance and security to the process.

Some of the fluid transients currently studied in the open literature can be summarized as: the flow start-up (Cawkwell and Charles, 1987; Chang et al., 1999; Davidson et al., 2004; Oliveira and Negrão, 2015; Vinay et al., 2007, 2006; Wachs et al., 2009), the pressure transmission (Oliveira et al., 2013, 2012) and the fluid hammer. Some extended works have been done in order to characterize and comprehend the behavior of non-Newtonian fluids for the flow start-up and the pressure transmission. As reported in the reviews of Steeter and Wylie (1974), Ghidaoui et al. (2005) and Bergant et al. (2006), the water hammer phenomenon is vastly studied, but few works try to understand the non-Newtonian fluid hammer.

Wahba (2013) evaluated the influence of the power-law index over the fluid hammer phenomenon by the use of a two-dimensional model. Tazraei et al. (2015) and Razraei and Riasi (2015) studied this problem by modeling the fluid through the Cross model and the flow as two-dimensional, the set of equations was solved with the method of

characteristics. Oliveira et al. (2015) studied the effect of viscoplastic fluid hammer by using an one-dimensional model solved by the method of characteristics.

Thus it can be concluded that few works that study the non-Newtonian hammer are found in the literature. They use different models to represent the behavior of the fluid and the flow is modeled as one and two-dimensional. It is known that the assumption of one or two-dimensional can influence over the results (Bergant et al., 2006; Ghidaoui et al., 2005). Nevertheless, the authors of the present paper have not found any work in the literature that compares 1D and 2D models. Therefore, the objective of this paper is to compare one and two-dimensional models for the non-Newtonian fluid hammer by considering the fluid as a power-law.

3. MATHEMATICAL MODELS

The fluid hammer problem can be represented by the fully developed flow from a reservoir at the inlet of the pipeline to the outlet where a sudden closure valve is placed. Figure 1 presents a schematic representation of the problem, the reservoir is considered large enough so the inlet pressure is constant, the pipeline which is completely rigid has a length of *l* and an inner diameter *d*. A fast closure valve is mounted at the outlet of the pipeline.

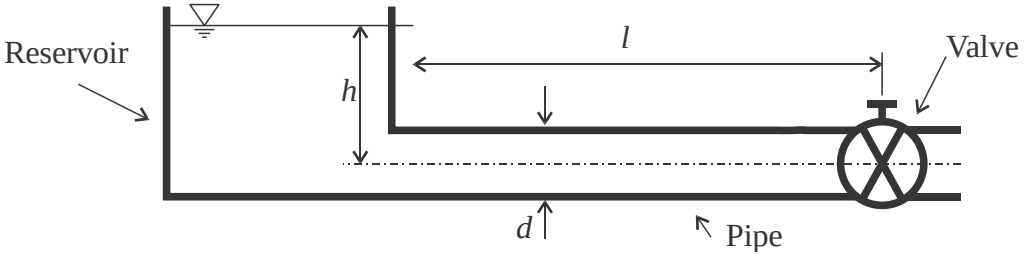

Figure 1. Schematic of the fluid hammer problem.

The non-Newtonian fluid hammer can be modeled by the mass and momentum balance equations. By considering the flow as axisymmetric, isothermal and weakly compressible, the Mach number as too small (Wahba, 2006) and that the isothermal compressibility, α, represents the relation of pressure and fluid density, these equations can be simplified and written as a function of the head pressure, *h*, as:

$$\frac{\partial h}{\partial t}+\frac{c^2}{g}\left[\frac{1}{r}\frac{\partial q}{\partial r}+\frac{\partial v_z}{\partial z}\right]=0 \tag{1}$$

$$\frac{\partial u}{\partial t}=-g\frac{\partial h}{\partial z}-\frac{1}{\rho r}\frac{\partial (r\tau)}{\partial r} \tag{2}$$

where *t* is the time, *c* is the wave speed, *g* is the gravity, *r* and *z* the radial and axial coordinates, $q = v_r r$ and v_z the radial and axial velocities, ρ is the fluid density and τ is the shear stress.

As the fluid is modeled as a power-law, the constitutive equation that represents its behavior is (Bird et al., 1987):

$$\tau=\eta\dot{\gamma}=k\dot{\gamma}^{n-1}\dot{\gamma} \tag{3}$$

where $\dot{\gamma} = \partial v_z/\partial r$ is the shear rate, $\eta = k(\partial v_z/\partial r)^n$ is the apparent viscosity, *k* is the consistency index and *n* is the power-law index.

3.1 1D Model

As the diameter is significantly lower than the length of the pipeline, the radius aspect, $\delta = d/l$, is small and then the flow can be considered one-dimensional. By integrating this equation in the cross section, considering that the mean velocity is $V_z=\int_A 2\pi v_r r dr \big/ A$ and the velocity profile is fully developed in all instants (shear stress varies linearly with the radial coordinate), the mass and momentum balance equations can be rewritten in the dimensionless form as:

$$\frac{\partial h^*}{\partial t^*}+\frac{1}{\alpha^*}\frac{\partial V_z^*}{\partial z^*}=0 \tag{4}$$

$$\frac{\partial V_z^*}{\partial t^*}=-\alpha^*\frac{\partial h^*}{\partial z^*}-\alpha^*\tau_{w,t}^* \tag{5}$$

where the superscript * represents dimensionless variables. These dimensionless variables are defined as: $h^* = \rho g h d/4l\tau_w$, $t^* = tc/l$, $V_z^* = V_z/c$, $z^* = z/l$ and $\tau_{w,t}^* = \tau_{w,t}/\tau_w$. The parameter α^* represents the ratio of viscous and inertia forces and can be written as:

$$\alpha^* = \frac{4\tau_w}{\rho c^2}\frac{L}{d} = \frac{32Ma^2}{\delta \,\mathrm{Re}} \tag{6}$$

The wall shear stress, $\tau_w = f\rho V_z^2/2$, can be written as a function of the friction factor, $f = 16/\mathrm{Re}$, so the momentum balance equation can be written in the final form:

$$\frac{\partial V_z^*}{\partial t^*} = -\alpha^*\frac{\partial h}{\partial z} - \frac{8\alpha^*}{Ma^n}V_z^{*n} \tag{7}$$

where $Ma = V_{z,in}/c$ is the Mach number.

Therefore, the dimensionless parameters that govern the one-dimensional model are the compressibility (α^*), the Mach number (Ma) and the power-law index (n).

The initial condition is of a fully developed fluid, so the initial velocity is the same in all axial position. As boundary conditions, the inlet pressure is constant, $h_{in}^* = 1$, and the outlet velocity is null, $V_{z,out}^* = 0$.

3.2 2D Model

By considering that the flow occurs for both radial and axial directions, the mass and momentum balance equations can be written in the dimensionless form as:

$$\frac{\partial h^*}{\partial t^*} + \frac{1}{\alpha^*\delta}\frac{1}{r^*}\frac{\partial q^*}{\partial r^*} + \frac{1}{\alpha^*}\frac{\partial v_z^*}{\partial z^*} = 0 \tag{8}$$

$$\frac{\partial v_z^*}{\partial t^*} = -\alpha^*\frac{\partial h^*}{\partial z^*} - \frac{1}{2^{n+2}}\frac{\alpha^*}{r^*}\frac{1}{Ma^n}\left(\frac{n}{1+3n}\right)^n\frac{\partial}{\partial r^*}\left[r^*\left(\frac{\partial v_z^*}{\partial r^*}\right)^n\right] \tag{9}$$

where $v_z^* = v_z/c$, $q^* = q/cd$ and $r^* = r/d$.

Therefore, the dimensionless parameters that govern the one-dimensional model are the compressibility (α^*), the radius aspect (δ), the Mach number (Ma) and the power-law index (n).

The initial condition is of a fully developed flow. The boundary conditions are: symmetric at the center, $\tau_c^* = 0$ and $q_c^* = 0$, no-slip at the wall, $v_{z,w}^* = 0$ and $q_w^* = 0$, constant inlet pressure, $h_{in}^* = 1$, and null outlet velocity, $v_{z,out}^* = 0$.

4. SOLUTION METHODOLOGY

4.1 1D Model

The mass and momentum balance equations for the 1D model, Eqs. (4) and (7), form a set of hyperbolical partial differential equations that can be solved by the method of characteristics (Wylie et al., 1993). By making a linear combination of these equations, a set of ordinary differential equations is obtained. So the dependent variables (V_z^* and h^*) can be written as a function of t^* and z^*. These equations are valid over the characteristics lines $dz^*/dt^* = \pm 1$:

$$C^+\begin{cases}\dfrac{dV_z^*}{dt^*} + \alpha^*\dfrac{dh^*}{dt^*} + \dfrac{8\alpha^*}{Ma^n}V_z^{*n} \\ \dfrac{dz^*}{dt^*} = +1\end{cases} \tag{8}$$

$$C^-\begin{cases}\dfrac{dV_z^*}{dt^*} - \alpha^*\dfrac{dh^*}{dt^*} + \dfrac{8\alpha^*}{Ma^n}V_z^{*n} \\ \dfrac{dz^*}{dt^*} = -1\end{cases} \tag{8}$$

Figure 2(a) illustrates the plot of these equations. The pipeline was divided in NZ parts with length Δz^* and the time step was computed as $\Delta t^* = \Delta z^*$. If the variables V_z^* and h^* are known at the positions i-1 and i+1, so the equations can be integrated over the characteristics line in order to obtain the variables V_z^* and h^* at the position i. This procedure is

iterative as the wall shear stress is a function of the velocity at the postion *i*. The convergence is achieved when the relative difference between the velocities calculated is inferior to 0.1%. Then the simulation progress to the next time until the desired time is reached.

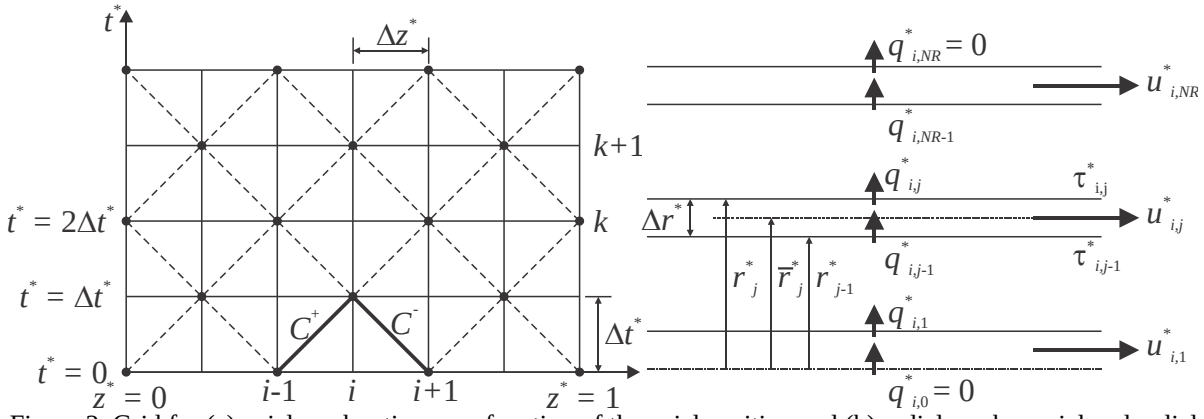

Figure 2. Grid for (a) axial mesh – time as a function of the axial position and (b) radial mesh – axial and radial velocities and shear stress as a function of the radial position.

4.2 2D Model

The same procedure is repeated for the 2D model, but as the problem is also dependent of the radial position, the mesh is two-dimensional. The characteristics lines for the 2D model are:

$$C^{+}\begin{cases}\dfrac{dv_z^*}{dt^*}+\alpha^*\dfrac{dh^*}{dt^*}+\dfrac{1}{\delta r^*}\dfrac{\partial q^*}{\partial r^*}+\dfrac{\alpha^*}{2^{n+2}Ma^n r^*}\left(\dfrac{n}{1+3n}\right)^n\dfrac{\partial}{\partial r^*}\left[r^*\left(\dfrac{\partial v_z^*}{\partial r^*}\right)^n\right]\\ \dfrac{dz^*}{dt^*}=+1\end{cases} \tag{8}$$

$$C^{-}\begin{cases}\dfrac{dv_z^*}{dt^*}-\alpha^*\dfrac{dh^*}{dt^*}-\dfrac{1}{\delta r^*}\dfrac{\partial q^*}{\partial r^*}+\dfrac{\alpha^*}{2^{n+2}Ma^n r^*}\left(\dfrac{n}{1+3n}\right)^n\dfrac{\partial}{\partial r^*}\left[r^*\left(\dfrac{\partial v_z^*}{\partial r^*}\right)^n\right]\\ \dfrac{dz^*}{dt^*}=-1\end{cases} \tag{8}$$

As for the 1D model, the plot of the characteristics lines is illustrated in Figure 2(a). Besides the axial mesh, a radial grid is also necessary to solve the set of ordinary equations. Then the pipeline is divided in *NR* parts of length Δr^*. Figure 2(b) presents the radial mesh. One can note that the grid of radial velocity and shear stress is displaced from the grid for axial velocity. That is done to avoid numerical errors due to the great number of variables at the same point. If the dependent variables (v_z^*, q^* and h^*) as a function of t^*, r^* and z^* are known at the points *i*-1 and *i*+1, the characteristics lines can be integrated in order to obtain the dependent variables at the point *i*. In doing so, two matrices as a function of the radial position for each axial position are formed: one for radial velocity and pressure and other for axial velocity (Zhao and Ghidaoui, 2003). These matrices are tridiagonal and can be solved by TDMA (Versteeg and Malalasekera, 2007). The procedure is repeated from the inlet to the outlet of the pipeline and then for the next time step until the simulation reaches the desired time.

5. VERIFICATION AND VALIDATION

The mesh was investigated in order to assure grid-independent results. It was concluded that a mesh of 200×640 (*NZ*×*NR*) was sufficient to provide the necessary independence. Then the models where compared to the experimental data of Holmboe and Rouleau (1967). In this work the water hammer phenomenon was studied via an experiment with a copper pipeline of inner diameter 25 mm and length of 36.09 m. The fluid used was a Newtonian oil (ρ = 876 kg.m^{-3}, c = 1324 m.s^{-1} and μ = 0.03484 Pa.s) which flowed with constant Reynolds number of 82. The experiment initiated with the sudden closure of the outlet vale.

Figure 3 shows the comparison of the measured results and the computed for the one and two-dimensional models. One can note that the 2D model presents good agreement with experimental data. Although the initial behavior of

experimental data can be well represented by the 1D model, the subsequent viscous dissipation and damping are not as close as the 2D model.

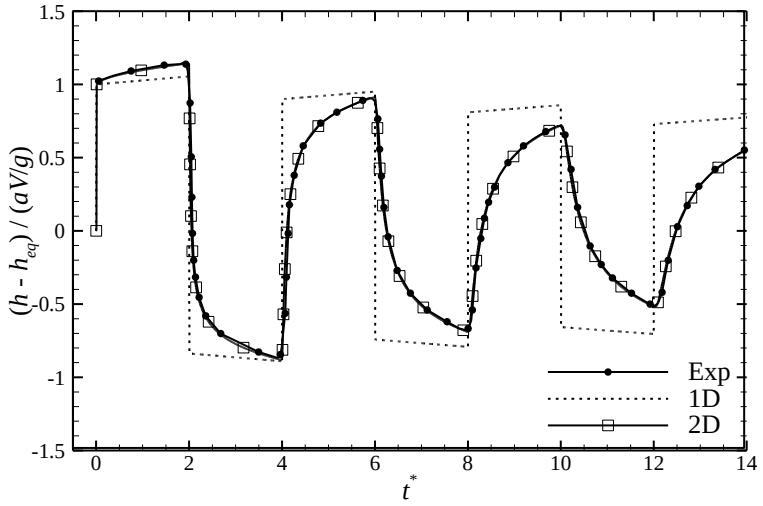

Figure 3. Comparison of the pressure evolution at the outlet valve for the present models and the experimental data of Holmboe and Rouleau (1967).

6. RESULTS AND DISCUSSION

The dimensionless parameters for the experiment of Holmboe and Rouleau (1967) are $\alpha^* = 5.469\times10^{-6}$, $\delta = 6.927\times10^{-4}$, $Ma = 9.853\times10^{-5}$ and $n = 1.0$. The comparison of the 1D and 2D models is going to be conducted by fixing the Mach number and the radius aspect, changing the power-law index in 0.6, 1.0 and 1.4 and varying the compressibility in $10\alpha^*$ and $100\alpha^*$.

Values of compressibility lower than α^* are not going to be addressed as in the previous section a divergence of the results of the models was already observed. And by analyzing Eqs (7) and (9), it can be concluded that lower values of the dimensionless compressibility increase the importance of the viscous term. Therefore, the difference caused by the consideration of a fully developed velocity profile in the one-dimensional model is amplified and emphasized. So the divergence of the results of the models will only increase.

Figure 4 presents the pressure head evolution at the valve for dimensionless compressibility of $10\alpha^*$ and $100\alpha^*$ and power-law indexes of 0.6, 1.0 and 1.4. For $10\alpha^*$ it can be observed that as the power-law index increases so does the number of oscillations prior to equilibrium. Thus higher dissipation is associated with pseudoplastic fluids. As it was seen in Figure 3, the 1D and 2D models results are quite different. The increase in pressure after the valve is closed ($t^* = 0$) is identical as it represents the Joukowski pressure (Joukowski, 1904). The following pressure rise (until $t^* = 2$) is distinct and the maximum pressure is smaller for the 1D model, so the 2D model is more dissipative. Figure 4(c) and (e) show that there is a delay in the wave propagation for the 2D model.

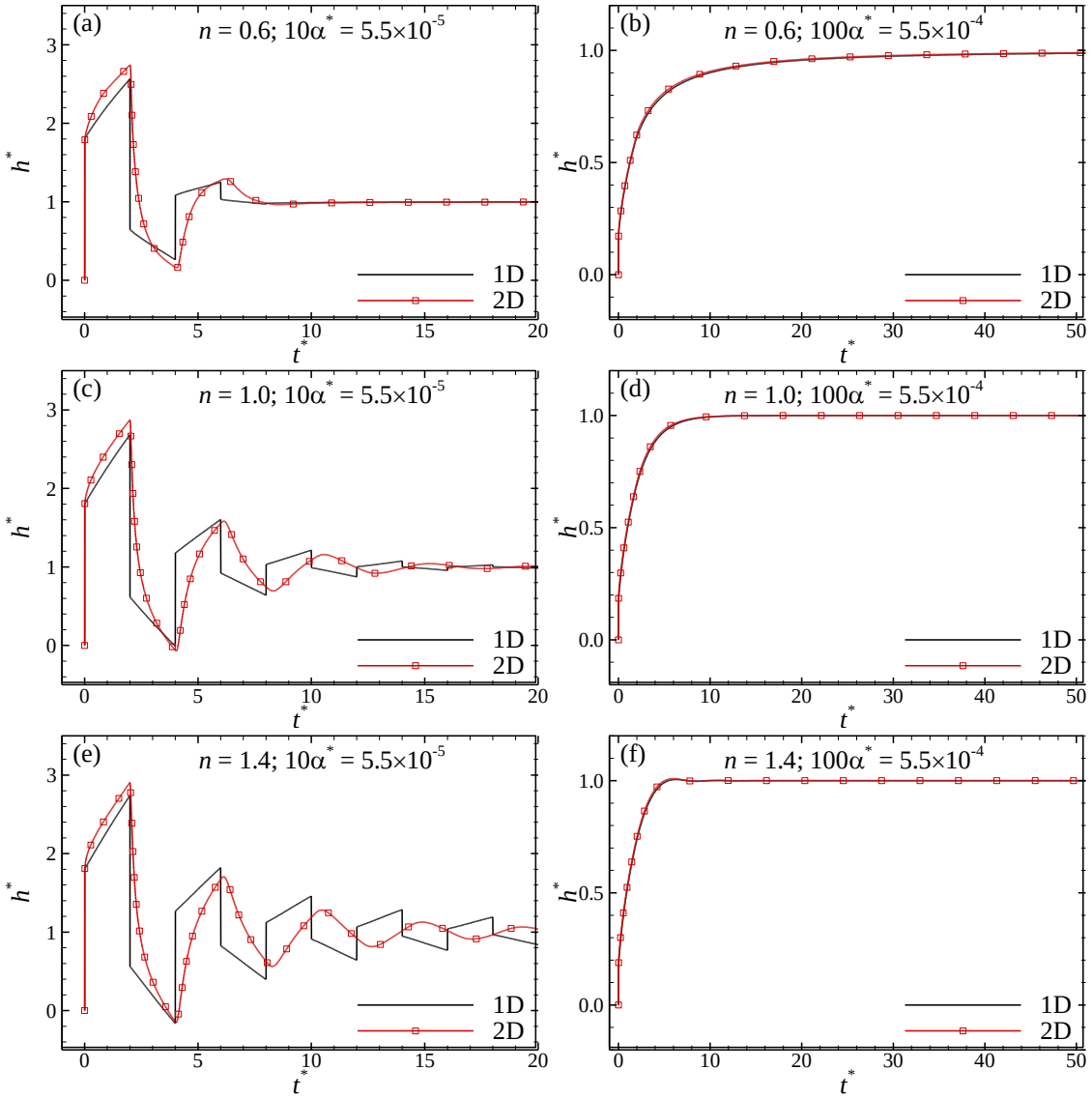

Figure 4. Comparison of the pressure evolution at the outlet valve for 1D and 2D models for different compressibilities and power-law indexes.

For $100\alpha^*$ the compressibility of the fluid increases and so does the dissipation. It can be observed in Figure 4 that when the power-law index increased the equilibrium is reached earlier. That once again shows that a high dissipation is associated to shear thinning effects. By comparing the 1D and 2D models, it can be concluded that in this high compressibility case the results are almost identical.

In order to understand better why there is less similarities in low compressibility cases, Figure 5 presents the velocity profile at the midpoint of the pipeline for the case $10\alpha^*$. One can note that the fluid returns close to the wall at $t = 1$. At $t = 2$ the shear thickening fluid has a maximum value for the return velocity that is close to the wall. For the shear thinning case the fluid also returns, but no maximum is found close to the wall. This is evidence that the higher the power-law index, the lower is the viscous dissipation. But the most important conclusion that can be drawn from Figure 5 is that the profile is not the one of a fully developed fluid. Thus this assumption is not valid for cases of low compressibility ($\alpha^* < 5\times10^{-4}$) and even though the results of the 1D model are close qualitatively and in equilibrium, the quantitative transient is not well represented.

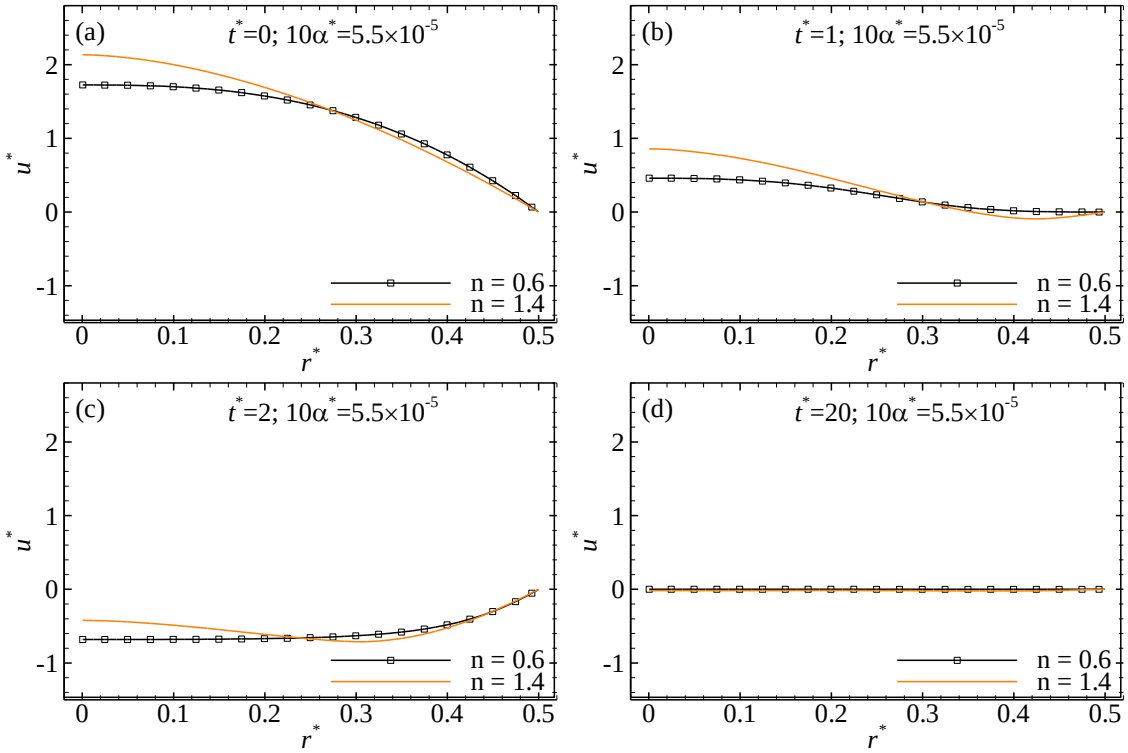

Figure 5. Comparison of the velocity profile of the 2D model at the midpoint of the pipeline for compressibility $10\alpha^* = 5.5\times10^{-5}$ at: (a) $t^* = 0$, (a) $t^* = 1$, (a) $t^* = 2$ and (a) $t^* = 20$.

For a higher dissipation ($100\alpha^*$) the velocity profiles are presented in Figure 6. The parabolic curve shape is evident since the time $t^* = 1$. Then, differently from the case of $10\alpha^*$, the assumption that the profile is fully developed at each time step is valid. Therefore the 1D model represents well both transient and equilibrium behavior.

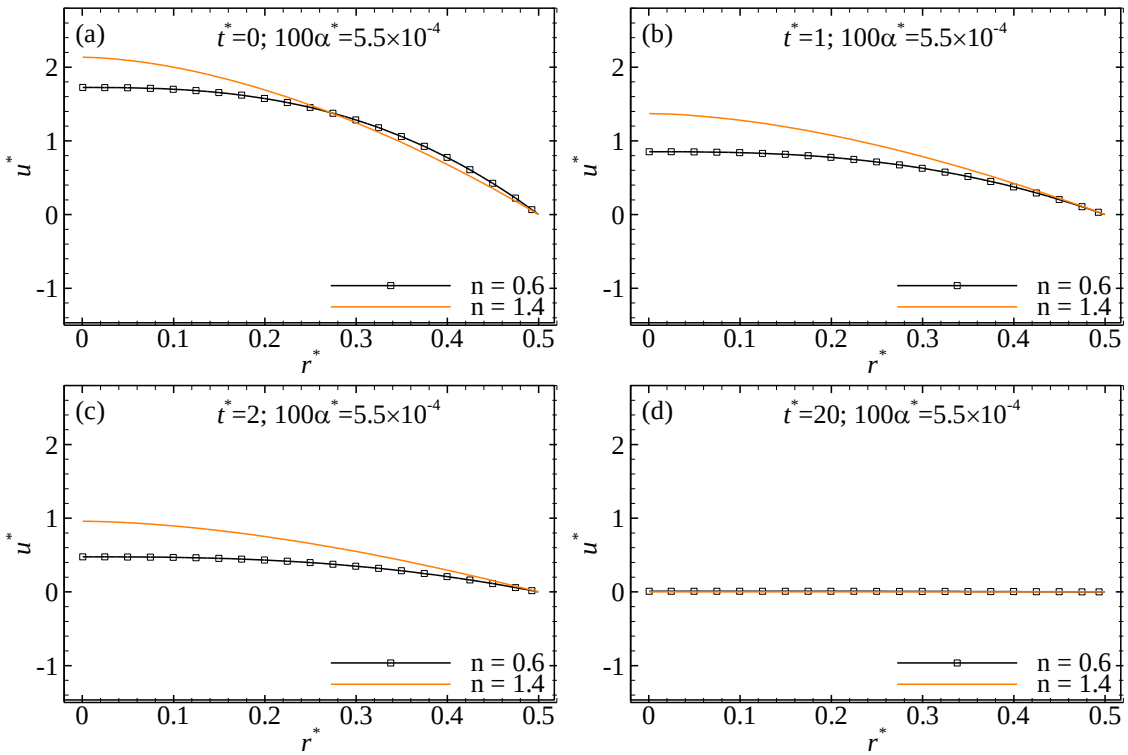

Figure 6. Comparison of the velocity profile of the 2D model at the midpoint of the pipeline for compressibility $100\alpha^* = 5.5\times10^{-4}$ at: (a) $t^* = 0$, (a) $t^* = 1$, (a) $t^* = 2$ and (a) $t^* = 20$.

7. CONCLUSION

The present paper compared one and two-dimensional models to simulate the non-Newtonian fluid hammer. The models were validated with the experimental data of Holmboe and Rouleau (1967). Then the dimensionless models were evaluated in terms of viscous dissipation and power-law index. It was observed that a low power-law index is associated with a higher viscous dissipation. For low compressibility cases, the results of the 1D model are quite different from the 2D model. Less dissipation and distortion is associated to the 1D model and the return of the fluid close to the wall is not verified. As the compressibility increases, both models present the same results.

Other parameters than influence over the compressibility are the Mach number and the aspect ratio. The Mach number is directly proportional and the aspect ratio is inversely proportional to the compressibility. So in medium and high speed flows and in long pipelines the results of the models are closer.

Therefore, it is necessary to analyze the compressibility of the fluid because only for values higher than 5×10^{-4} (high dissipation) the problem can be modeled as one-dimensional. Otherwise, the assumption of fully developed fluid at each time step is not valid and the transient is not well represented.

8. ACKNOWLEDGEMENTS

The authors acknowledge the financial support of PETROBRAS S/A (TC 0050.0070318.11.9), CNPq (Process: 487091/2013-2), CAPES, FINEP, PRH-ANP/MCT (PRH-ANP/MCTI no. 10-C) and PFRH/PETROBRAS (6000.0067933.11.4 and 6000.0082166.13.4).

9. REFERENCES

Bergant, A., Simpson, A.R., Tijsseling, A.S., 2006. Water hammer with column separation: A historical review. J. Fluids Struct. 22, 135–171. doi:10.1016/j.jfluidstructs.2005.08.008

Bird, R.B., Armstrong, R.C., Hassager, O., 1987. Dynamics of Polymeric Liquids Vol 1 Fluid Mechanics.

Cawkwell, M.G., Charles, M.E., 1987. An improved model for start-up of pipelines containing gelled crude oil. J. Pipelines 7, 41–52.

Chang, C., Nguyen, Q.D., Rønningsen, H.P., 1999. Isothermal start-up of pipeline transporting waxy crude oil. J. Nonnewton. Fluid Mech. 87, 127–154. doi:10.1016/S0377-0257(99)00059-2

Davidson, M.R., Dzuy Nguyen, Q., Chang, C., Rønningsen, H.P., 2004. A model for restart of a pipeline with compressible gelled waxy crude oil. J. Nonnewton. Fluid Mech. 123, 269–280. doi:10.1016/j.jnnfm.2004.09.007

Ghidaoui, M.S., Zhao, M., McInnis, D.A., Axworthy, D.H., 2005. A Review of Water Hammer Theory and Practice. Appl. Mech. Rev. 58, 49. doi:10.1115/1.1828050

Holmboe, E.L., Rouleau, W.T., 1967. The Effect of Viscous Shear on Transients in Liquid Lines. J. Basic Eng. 89, 174. doi:10.1115/1.3609549

Joukowski, N., 1904. Water hammer. Proc. Am. Water Work. Assoc. 24, 341–424.

Oliveira, G.M. de, Franco, A.T., Negrão, C.O.R., Martins, A.L., Silva, R.A., 2013. Modeling and validation of pressure propagation in drilling fluids pumped into a closed well. J. Pet. Sci. Eng. 103, 61–71. doi:10.1016/j.petrol.2013.02.012

Oliveira, G.M., Franco, A.T., Negrão, C.O.R., 2015. Mathematical Model for Viscoplastic Fluid Hammer. J. Fluids Eng. 138, 011301. doi:10.1115/1.4031001

Oliveira, G.M., Negrão, C.O.R., 2015. The effect of compressibility on flow start-up of waxy crude oils. J. Nonnewton. Fluid Mech. 220, 137–147. doi:10.1016/j.jnnfm.2014.12.010

Oliveira, G.M., Negrão, C.O.R., Franco, A.T., 2012. Pressure transmission in Bingham fluids compressed within a closed pipe. J. Nonnewton. Fluid Mech. 169-170, 121–125. doi:10.1016/j.jnnfm.2011.11.004

Streeter, V.L., Wylie, E.B., 1974. Waterhammer and Surge Control. Annu. Rev. Fluid Mech. 6, 57–73. doi:10.1146/annurev.fl.06.010174.000421

Tazraei, P., Riasi, A., 2015. Quasi-Two-Dimensional Numerical Analysis of Fast Transient Flows Considering Non-Newtonian Effects. J. Fluids Eng. 138, 011203. doi:10.1115/1.4031093

Tazraei, P., Riasi, A., Takabi, B., 2015. The influence of the non-Newtonian properties of blood on blood-hammer through the posterior cerebral artery. Math. Biosci. 264, 119–127. doi:10.1016/j.mbs.2015.03.013

Versteeg, H.K., Malalasekera, W., 2007. Introduction: Computational Fluid Dynamics.

Vinay, G., Wachs, A., Agassant, J.-F., 2006. Numerical simulation of weakly compressible Bingham flows: The restart of pipeline flows of waxy crude oils. J. Nonnewton. Fluid Mech. 136, 93–105. doi:10.1016/j.jnnfm.2006.03.003

Vinay, G., Wachs, A., Frigaard, I., 2007. Start-up transients and efficient computation of isothermal waxy crude oil flows. J. Nonnewton. Fluid Mech. 143, 141–156. doi:10.1016/j.jnnfm.2007.02.008

Wachs, A., Vinay, G., Frigaard, I., 2009. A 1.5D numerical model for the start up of weakly compressible flow of a

viscoplastic and thixotropic fluid in pipelines. J. Nonnewton. Fluid Mech. 159, 81–94. doi:10.1016/j.jnnfm.2009.02.002

Wahba, E.M., 2013. Non-Newtonian fluid hammer in elastic circular pipes: Shear-thinning and shear-thickening effects. J. Nonnewton. Fluid Mech. 198, 24–30. doi:10.1016/j.jnnfm.2013.04.007

Wahba, E.M., 2006. Runge–Kutta time-stepping schemes with TVD central differencing for the water hammer equations. Int. J. Numer. Methods Fluids 52, 571–590. doi:10.1002/fld.1188

Wylie, E.B., Streeter, V.L., Suo, L., 1993. Fluid transients in systems.

Zhao, M., Ghidaoui, M.S., 2003. Efficient Quasi-Two-Dimensional Model for Water Hammer Problems. J. Hydraul. Eng. 129, 1007–1013. doi:10.1061/(ASCE)0733-9429(2003)129:12(1007)

10. RESPONSIBILITY NOTICE

The authors are the only responsible for the printed material included in this paper.